



RESEARCH PAPER

# The response of mesophyll conductance to short-term variation in CO<sub>2</sub> in the C<sub>4</sub> plants *Setaria viridis* and *Zea mays*

Nerea Ubierna<sup>1</sup>, Anthony Gandin<sup>1,†</sup> and Asaph B. Cousins<sup>1,\*</sup>

<sup>1</sup> School of Biological Sciences, Molecular Plant Sciences, Washington State University, Pullman, Washington 99164–4236, USA

<sup>†</sup> Present address: Université de Lorraine, Faculté des Sciences et Techniques, Ecologie et Ecophysiologie Forestières, F54506 Vandoeuvre Les Nancy, France.

\* Correspondence: [acousins@wsu.edu](mailto:acousins@wsu.edu)

Received 26 March 2017; Editorial decision 4 December 2017; Accepted 10 January 2018

Editor: Susanne von Caemmerer, Australian National University, Australia

## Abstract

Mesophyll conductance ( $g_m$ ) limits rates of C<sub>3</sub> photosynthesis but little is known about its role in C<sub>4</sub> photosynthesis. If  $g_m$  were to limit C<sub>4</sub> photosynthesis, it would likely be at low CO<sub>2</sub> concentrations ( $pCO_2$ ). However, data on C<sub>4</sub>- $g_m$  across ranges of  $pCO_2$  are scarce. We describe the response of C<sub>4</sub>- $g_m$  to short-term variation in  $pCO_2$ , at three temperatures in *Setaria viridis*, and at 25 °C in *Zea mays*. Additionally, we quantified the effect of finite  $g_m$  calculations of leakiness ( $\phi$ ) and the potential limitations to photosynthesis imposed by stomata, mesophyll, and carbonic anhydrase (CA) across  $pCO_2$ . In both species,  $g_m$  increased with decreasing  $pCO_2$ . Including a finite  $g_m$  resulted in either no change or increased  $\phi$  compared with values calculated with infinite  $g_m$  depending on whether the observed <sup>13</sup>C discrimination was high (*Setaria*) or low (*Zea*). Post-translational regulation of the maximal PEP carboxylation rate and PEP regeneration limitation could influence estimates of  $g_m$  and  $\phi$ . At  $pCO_2$  below ambient, the photosynthetic rate was limited by CO<sub>2</sub> availability. In this case, the limitation imposed by the mesophyll was similar or slightly lower than stomata limitation. At very low  $pCO_2$ , CA further constrained photosynthesis. High  $g_m$  could increase CO<sub>2</sub> assimilation at low  $pCO_2$  and improve photosynthetic efficiency under situations when CO<sub>2</sub> is limited, such as drought.

**Keywords:** A-C<sub>i</sub> curves, carbonic anhydrase, CO<sub>2</sub>, C<sub>4</sub> photosynthesis, diffusional limitations, *in-vitro* V<sub>pmax</sub>, leakiness, mesophyll conductance, *Setaria viridis*, *Zea mays*.

## Introduction

In C<sub>4</sub> plants photorespiration is reduced by concentrating CO<sub>2</sub> around Rubisco (ribulose 1,5-bisphosphate carboxylase/oxygenase) (Edwards and Walker, 1983; Hatch, 1987; Sage, 2004). In Kranz-type C<sub>4</sub> plants this is achieved with a compartmentalized two-carboxylation process: (1) in the cytosol of mesophyll cells, bicarbonate (HCO<sub>3</sub><sup>-</sup>) and phosphoenolpyruvate are fixed into four-carbon acids by phosphoenolpyruvate carboxylase (PEPC) (Hatch *et al.*, 1967); and (2) in chloroplasts of the bundle-sheath cells the concentrated CO<sub>2</sub> released from the decarboxylation of these acids is fixed by Rubisco.

Mesophyll conductance ( $g_m$ ) describes the movement of CO<sub>2</sub> from stomata across the intercellular spaces to the sites of first carboxylation, which are the chloroplast stroma or mesophyll cytosol in C<sub>3</sub> and C<sub>4</sub> species, respectively (Evans and von Caemmerer, 1996). There is extensive research describing  $g_m$  in C<sub>3</sub> species; however, C<sub>4</sub>- $g_m$  is poorly understood because it is difficult to estimate. Traditionally  $g_m$  was assumed to be larger in C<sub>4</sub> compared to C<sub>3</sub> species, but most recent studies suggest that values for C<sub>4</sub>- $g_m$  correspond to higher-end C<sub>3</sub>- $g_m$  reports, and that C<sub>4</sub>- $g_m$  reacts similarly to C<sub>3</sub>- $g_m$  with

regards to variation in factors such as leaf age and temperature (Barbour *et al.*, 2016; Osborn *et al.*, 2017; Ubierna *et al.*, 2017). If  $C_4$ - $g_m$  is lower than previously thought, that could affect derivations of other key parameters such as leakiness ( $\phi$ , the proportion of C fixed by PEPC that subsequently leaks out the bundle-sheath cells). Leakiness cannot be directly measured and is commonly estimated from observations and models of  $^{13}\text{C}$  discrimination ( $\Delta^{13}\text{C}$ ) (Farquhar, 1983; Farquhar and Cernusak, 2012). Historically,  $g_m$  is generally assumed to be infinite when solving for  $\phi$  from  $\Delta^{13}\text{C}$ ; however, this simplification and estimates of  $\phi$  would be compromised if  $g_m$  is finite and low.

Mesophyll conductance has long been recognized as a significant limitation for  $C_3$  photosynthesis (Evans, 1983; Evans *et al.*, 1986; Evans and Terashima, 1988), limiting photosynthesis as much as stomatal conductance (Warren, 2008). It is unclear if  $g_m$  limits  $C_4$  photosynthesis as the reduction of photorespiration achieved by the  $\text{CO}_2$ -concentrating mechanism saturates  $C_4$  photosynthesis at ambient  $p\text{CO}_2$ . If  $g_m$  were to limit  $C_4$  photosynthesis, it would likely only be at very low  $p\text{CO}_2$ . However, not much is known about the variation of  $C_4$ - $g_m$  with  $p\text{CO}_2$ . In the  $C_4$  grass *Setaria viridis*,  $g_m$  derived with the  $^{18}\text{O}$  discrimination ( $\Delta^{18}\text{O}$ ) method increased as  $p\text{CO}_2$  decreased, although the variation was not significant (Osborn *et al.*, 2017). Some reports have shown that in  $C_3$  species  $g_m$  increases with short-term exposure to decreasing  $p\text{CO}_2$  (Bongi and Loreto, 1989; Loreto *et al.*, 1992; Flexas *et al.*, 2007, 2008; Hassiotou *et al.*, 2009; Bunce, 2010; Douthe *et al.*, 2011; Tazoe *et al.*, 2011). However, others have suggested that  $C_3$ - $g_m$  is insensitive to changes in  $p\text{CO}_2$  (Loreto *et al.*, 1992; Tazoe *et al.*, 2009). It has been hypothesized that the observed  $C_3$ - $g_m$  response to  $p\text{CO}_2$  might result from a significant chloroplast resistance (Tholen and Zhu, 2011; Tholen *et al.*, 2012) or artifacts in the calculations (Gu and Sun, 2014).

In  $C_4$  plants,  $g_m$  has been estimated with the  $\Delta^{18}\text{O}$  method (Gillon and Yakir, 2000a, 2000b; Barbour *et al.*, 2016; Osborn *et al.*, 2017; Ubierna *et al.*, 2017) and the *in vitro* maximal PEP carboxylation rate ( $V_{\text{pmax}}$ ) method (Ubierna *et al.*, 2017). The latter method solves for the  $p\text{CO}_2$  in the mesophyll cells ( $C_m$ ) needed to simultaneously match modeled and measured rates of  $\text{CO}_2$  assimilation and  $\Delta^{13}\text{C}$  when the models are parameterized with *in vitro*  $V_{\text{pmax}}$ , as determined in a crude leaf extract. Values derived for  $g_m$  with the  $\Delta^{18}\text{O}$  and *in vitro*  $V_{\text{pmax}}$  methods were similar in two  $C_4$  species measured over a range of temperatures (Ubierna *et al.*, 2017). The *in vitro*  $V_{\text{pmax}}$  method also allows the implementation of two modeling alternatives: carbonic anhydrase (CA)-saturated and CA-limited. They differ in the calculation of PEP carboxylation rate as a function of  $\text{CO}_2$  or  $\text{HCO}_3^-$  for the CA-saturated and -limited scenarios, respectively. Ubierna *et al.* (2017) found no difference between CA-limited and CA-saturated estimates of  $g_m$  at ambient  $p\text{CO}_2$ , but CA limitation is expected at low  $p\text{CO}_2$ .

In this study, we calculated  $g_m$  using the *in vitro*  $V_{\text{pmax}}$  method across a range of  $p\text{CO}_2$  in two  $C_4$  grasses, one economically important (*Zea mays*) and the other the adopted model system for studying  $C_4$  photosynthesis (*S. viridis*). Measurements were performed at three temperatures (10, 25,

and 40 °C) in *Setaria* and at 25 °C in *Zea*. Our objectives were to: (1) describe the response of  $C_4$ - $g_m$  to short-term variation in  $p\text{CO}_2$ ; (2) evaluate the impact of disequilibrium between  $\text{CO}_2$  and  $\text{HCO}_3^-$  at a range of  $p\text{CO}_2$  and temperatures; (3) investigate if  $g_m$  represents a limitation to  $C_4$  photosynthesis across  $p\text{CO}_2$ ; and (4) assess the impact of finite  $g_m$  on  $\phi$  calculations.

## Materials and methods

### Plant material

Seeds of *Z. mays* (var. Trucker's Favorite, Victory Seed Company, Oregon, USA) were grown in a greenhouse supplemented with artificial lighting at the School of Biological Sciences at Washington State University, Pullman, WA (USA) during August to October 2011. Seeds of *S. viridis* (A-010) were grown in a controlled environment growth chamber (Enconair Ecological GC-16) in 2013. Plants used for measurements were 4 and 6 weeks old for *Zea* and *Setaria*, respectively. *Zea* was fertilized with 17-3-6 NPK and weekly additions of 4 g l<sup>-1</sup> solution of 10% Fe-DPTA (Sprint 330, Becker Underwood, IA, USA). *Setaria* was treated weekly with Peters 20-20-20 (J. R. Peters, Inc., Allentown, PA, USA). For all plants, the photon flux density was  $\geq 500 \mu\text{mol m}^{-2} \text{s}^{-1}$ , the day length was 14 h, and the temperature was 25–28/20–25 °C for day/night.

### Coupled gas exchange and isoflux measurements

The system used for measurements has been described in detail in Ubierna *et al.* (2013, 2017). Briefly, a LI-6400XT open gas exchange system assembled with a 6400-22L conifer chamber fitted with a LI-6400-18 RGB light source (Li-Cor, Lincoln, NE, USA) was coupled with a tunable-diode laser absorption spectroscope (TDLAS, TGA 200A, Campbell Scientific, Inc. Logan, UT, USA). The entire gas exchange system was placed in a growing cabinet (Percival Scientific, Perry, IA), where the temperature was varied to match leaf temperature ( $T_L$ ) settings. The TDLAS data were calibrated with the concentration series method (Tazoe *et al.*, 2011; Ubierna *et al.*, 2013) using two calibration gases, one measured at different  $[\text{CO}_2]$  that spanned the gas exchange reference and sample lines. Each measurement cycle included five to seven TDLAS sequences of zero air, calibration gases, reference, and sample lines measured for 40 s each. Data from the last three sequences were averaged and used for calculations.

Young fully-expanded leaves of *Setaria* and *Zea* were acclimated for ~1 h with chamber conditions of  $C_a$  (ambient  $\text{CO}_2$  supply to the chamber)  $\approx 35$  Pa, 21%  $\text{O}_2$ , and photosynthetically active radiation (PAR)  $= 2000 \mu\text{mol m}^{-2} \text{s}^{-1}$ . Then,  $C_a$  was varied in steps, and gas and  $^{13}\text{C}$  isotopic exchange were measured simultaneously. In *Setaria* ( $n=4$ )  $C_a$  was set at 5, 7, 10, 12, 14, 19, 28, 38, 56, and 93 Pa, and measurements were performed at  $T_L=10, 25$  and 40 °C. In *Zea* ( $n=3$ ),  $C_a$  was set at 9, 14, 19, 35, 56, 84, and 112 Pa, and  $T_L=25$  °C. In both species the measurements were performed in the sequence ambient – low – ambient – high  $p\text{CO}_2$ .

### Enzyme-limited $C_4$ photosynthesis model for CA-limited or CA-saturated conditions

The enzyme-limited  $C_4$  photosynthesis rate is (von Caemmerer, 2000):

$$A = \frac{-b - \sqrt{b^2 - 4ac}}{2a}, \quad \text{Eqn 1}$$

where:

$$a = 1 - \frac{\alpha K_c}{u_{cc} K_o}, \quad \text{Eqn 2}$$

$$b = - \left[ \frac{V_p - R_m + g_{bs} C_m + V_{cmax} - R_d}{+g_{bs} K_c \left(1 + \frac{O_m}{K_o}\right) + \frac{\alpha}{u_{oc}} \left(\gamma^* V_{cmax} + R_d \frac{K_c}{K_o}\right)} \right], \quad \text{Eqn 3}$$

$$c = (V_{cmax} - R_d)(V_p - R_m + g_{bs} C_m) - V_{cmax} g_{bs} \gamma^* O_m - R_d g_{bs} K_c \left(1 + \frac{O_m}{K_o}\right), \quad \text{Eqn 4}$$

where  $\alpha$  ( $= 0$ ) is the fraction of PSII activity in the bundle-sheath cells (von Caemmerer, 2000);  $u_{oc}$  is the ratio of O<sub>2</sub> and CO<sub>2</sub> diffusivities and solubilities, 0.047 at 25 °C but variable with temperature (Yin et al., 2016);  $g_{bs}$  is the bundle-sheath conductance, 0.0164  $\mu\text{mol m}^{-2} \text{s}^{-1} \text{Pa}^{-1}$  (Ubierna et al., 2013) or variable;  $O_m$  is the O<sub>2</sub> partial pressure in the mesophyll (19.5 kPa, which corresponds to 21%);  $R_d$  is the non-photorespiratory CO<sub>2</sub> released in the dark, assumed to equal measured rates of dark respiration after 30 min of dark adaptation, which at 25 °C were 1.89 and 1.06  $\mu\text{mol m}^{-2} \text{s}^{-1}$  in *Zea* and *Setaria*, respectively, but were also measured at each temperature;  $R_m$  is the mesophyll mitochondrial respiration rate,  $R_m = 0.5R_d$  (von Caemmerer, 2000);  $\gamma^*$  is half of the reciprocal of Rubisco specificity, and equals  $0.5/S_{C/O}$  (von Caemmerer, 2000), where  $S_{C/O}$  is the Rubisco CO<sub>2</sub>/O<sub>2</sub> specificity.  $K_C$  and  $K_O$  are the Michaelis–Menten constants of Rubisco for CO<sub>2</sub> and O<sub>2</sub>, respectively.  $S_{C/O}$ ,  $K_C$ , and  $K_O$  were determined *in vitro* at 25 °C in *Zea* ( $S_{C/O} = 2147 \text{ Pa Pa}^{-1}$ ,  $K_C = 96 \text{ Pa}$ ,  $K_O = 49\,683 \text{ Pa}$ ; R.A. Boyd, Washington State University, pers. comm.) and *Setaria* ( $S_{C/O} = 1310 \text{ Pa Pa}^{-1}$ ,  $K_C = 121 \text{ Pa}$ ,  $K_O = 29\,200 \text{ Pa}$ ; Boyd et al., 2015). Their values at different temperatures were obtained using the temperature functions of Boyd et al. (2015). For  $V_{cmax}$  (maximal Rubisco carboxylation rate) we used *in vivo* values calculated as described in Ubierna et al. (2017) or as specified otherwise. The calculation of  $C_m$  ( $p\text{CO}_2$  in the mesophyll cells) will be discussed subsequently.

CA-saturated and CA-limited models differ as follows.

(1) The calculation of PEP carboxylation rate ( $V_p$ ):

$$V_p = \left\{ \begin{array}{l} \text{CA saturated} \rightarrow \frac{C_m V_{pmax}}{C_m + K_p} \\ \text{CA limited} \rightarrow \frac{[\text{HCO}_3^-] V_{pmax}}{[\text{HCO}_3^-] + K_p} \end{array} \right\}, \quad \text{Eqn 5}$$

where the maximal PEP carboxylation rate ( $V_{pmax}$ ) was measured *in vitro* at 25 °C in *Zea* (184  $\mu\text{mol m}^{-2} \text{s}^{-1}$ , R. A. Boyd, pers. comm.) and in *Setaria* (450  $\mu\text{mol m}^{-2} \text{s}^{-1}$ , Boyd et al. 2015) and varied with temperature as described in Boyd et al. (2015). For all species, the Michaelis–Menten constant of PEPC for CO<sub>2</sub> ( $K_p$ ) was modeled with the temperature response and value at 25 °C (60.5  $\mu\text{M HCO}_3^-$ ) from Boyd et al. (2015). The  $[\text{HCO}_3^-]$  was calculated as previously discussed (Jenkins et al., 1989; Hatch and Burnell, 1990; Boyd et al., 2015); for details see Ubierna et al. (2017).

If the rate of PEP regeneration is limiting, then  $V_p$  is (von Caemmerer, 2000):

$$V_p = \min(V_p \text{ calculated with Eqn 5}, V_{pr}), \quad \text{Eqn 6}$$

where  $V_{pr}$  is the PEP regeneration rate (Peisker, 1986; Peisker and Henderson, 1992). We arbitrarily set  $V_{pr}$  to 64 and 59  $\mu\text{mol m}^{-2} \text{s}^{-1}$  in *Setaria* and *Zea*, respectively, which corresponded to twice the maximum measured net assimilation rate,  $A$ .

(2) The calculation of the ratio  $V_p/V_h$ , where  $V_h$  is hydration rate:

$$\frac{V_p}{V_h} = \left\{ \begin{array}{l} \text{CA saturated} \rightarrow 0 \\ \text{CA limited} \rightarrow \frac{V_p}{C_m K_{CA}} \end{array} \right\}, \quad \text{Eqn 7}$$

where  $K_{CA}$  is the rate constant of CA for CO<sub>2</sub>, that at 25 °C was 65.5 and 124  $\mu\text{mol m}^{-2} \text{s}^{-1} \text{Pa}^{-1}$  in *Zea* and *Setaria*, respectively (R.A. Boyd pers. comm., Boyd et al., 2015), varying with temperature as described in Boyd et al. (2015).

#### Measurements and models of discrimination

The observed photosynthetic discrimination against <sup>13</sup>C ( $\Delta^{13}_{obs}$ ) is calculated as (Evans et al., 1986):

$$\Delta^{13}_{obs} = \frac{\frac{C_{in}}{C_{in} - C_{out}} (\delta_{out} - \delta_{in})}{1 + \delta_{out} - \frac{C_{in}}{C_{in} - C_{out}} (\delta_{out} - \delta_{in})}, \quad \text{Eqn 8}$$

where  $C$  and  $\delta$  are the <sup>12</sup>CO<sub>2</sub> mol fraction and the  $\delta^{13}\text{C}$  of the CO<sub>2</sub>, respectively, in dry air in and out the chamber.

The theoretical model for  $\Delta^{13}\text{C}$  is (Farquhar and Cernusak, 2012):

$$\Delta^{13}_{theo} = \frac{1}{1-t} \left[ a_b \frac{C_a - C_L}{C_a} + a_s \frac{C_L - C_i}{C_a} \right] + \frac{1+t}{1-t} \left[ a_m \frac{C_i - C_m}{C_a} + \frac{b_4 + \phi \left( \frac{b_3 C_{bs} - s}{C_{bs} - C_m} \right) \frac{C_m}{C_a}}{1 + \frac{\phi C_m}{C_{bs} - C_m}} \right]. \quad \text{Eqn 9}$$

Values and calculations of the variables included in this equation have been discussed before (i.e. Ubierna et al., 2017) and can also be found in Supplementary Methods S1 at JXB online.

#### Calculation of mesophyll conductance ( $g_m$ )

Following Fick's law of diffusion:

$$g_m = \frac{A}{C_i - C_m}, \quad \text{Eqn 10}$$

where the  $C_m$  is calculated for two case scenarios, CA-saturated and CA-limited, resulting in CA-sat  $g_m$  and CA-lim  $g_m$  values. In both cases,  $C_m$  is derived with the *in vitro*  $V_{pmax}$  method as the  $C_m$  that needs to be combined with *in vitro*  $V_{pmax}$  to match measurements and predictions of  $A$  and  $\Delta^{13}\text{C}$  (Eqns 1, 9); details on these calculations have been provided in Ubierna et al. (2017). The CA-sat and CA-lim options are introduced through the calculation of  $V_p$  and  $V_p/V_h$  (Eqns 5–7).

#### Limitations to photosynthesis

To calculate the limitation on CO<sub>2</sub> assimilation by either finite stomatal conductance ( $L_s$ ), by mesophyll conductance ( $L_m$ ), or by carbonic anhydrase ( $L_{CA}$ ), we adapted to C<sub>4</sub> photosynthesis an approach previously used for C<sub>3</sub> photosynthesis. This compares  $A$  when all conductances are finite with the  $A$  estimated assuming that the conductance related with the limitation of interest is infinite (Farquhar and Sharkey, 1982; Warren et al., 2003). In all cases  $A$  was calculated with Eqn 1 and assuming:

- $A_{all}$  (expected  $A$  with all limitations,  $\approx$  measured photosynthetic rate): finite  $g_s$  and  $g_m$ , CA-lim model.
- $A_s$  (expected  $A$  if there were no stomatal limitations): infinite  $g_s$  ( $C_i = C_a$ ), finite  $g_m$ , CA-lim model.
- $A_m$  (expected  $A$  if there were no mesophyll limitations): infinite  $g_m$  ( $C_m = C_i$ ),  $g_s$  as measured, CA-lim model.
- $A_{CA}$  (expected  $A$  if there were no CA limitations):  $g_s$  as measured,  $g_m$  finite, CA-sat model.

Then  $L_s$ ,  $L_m$ , and  $L_{CA}$  were calculated as:

$$L_s = 100 \times \frac{A_s - A_{all}}{A_s}, \quad \text{Eqn 11}$$

$$L_m = 100 \times \frac{A_m - A_{all}}{A_m}, \quad \text{Eqn 12}$$

$$L_{CA} = 100 \times \frac{A_{CA} - A_{all}}{A_{CA}}. \quad \text{Eqn 13}$$

Calculation of leakiness ( $\phi$ )

The  $C_4$  photosynthesis model (von Caemmerer, 2000) calculates  $\phi$  as:

$$\phi = \frac{g_{bs}(C_{bs} - C_m)}{V_p}, \quad \text{Eqn 14}$$

where  $C_{bs}$ , the  $pCO_2$  in the bundle-sheath cells, is (von Caemmerer, 2000):

$$C_{bs} = \frac{\gamma^* O_s + K_c \left(1 + \frac{O_s}{K_o}\right) \left(\frac{A + R_d}{V_{cmax}}\right)}{1 - \frac{A + R_d}{V_{cmax}}} = C_m + \frac{V_p - A - R_m}{g_{bs}}, \quad \text{Eqn 15}$$

where  $O_s$  is the  $O_2$  partial pressure in the bundle-sheath cells.

From  $\Delta^{13}C$  (Eqn 9),  $\phi$  is solved as:

$$\phi = \frac{C_{bs} - C_m}{C_m} \times \frac{\Delta^{13}_{obs} (1-t) C_a - \bar{a} (C_a - C_i)}{(1+t) [b_3 C_{bs} - s (C_{bs} - C_m) + a_m (C_i - C_m)] + \bar{a} (C_a - C_i) - C_a \Delta^{13}_{obs} (1-t)}, \quad \text{Eqn 16}$$

where  $b_3$  (combined effects of Rubisco fractionation, and fractionations associated with respiration and photorespiration) and  $b_4$  (combined fractionation during PEP carboxylation, hydration, and respiration) are calculated as (Farquhar, 1983; Cousins *et al.*, 2006):

$$b_3 \equiv b_3' - \frac{eR_d}{V_c} - \frac{0.5fV_o}{V_c}, \quad \text{Eqn 17}$$

$$b_4 = b_4' \left(1 - \frac{V_p}{V_h}\right) + (e_s + h) \frac{V_p}{V_h} - \frac{eR_m}{V_p}. \quad \text{Eqn 18}$$

A description of other variables included in Eqns 16–19 can be found in [Supplementary Methods S1](#).

To evaluate the effect of  $g_m$  on calculations of  $\phi$  we implemented four model scenarios, which differed in values for  $g_m$ , calculation of  $V_p$ , or constraints imposed. Model 1 used *in vitro*  $V_{pmax}$  and  $g_m$  finite and equal to the values for CA-lim  $g_m$  presented in the Results; Model 2 used *in vivo*  $V_{pmax}$  and  $g_m$  infinite; Model 3 was the same as Model 1 but the solution was only constrained by  $A$  and not  $\Delta^{13}C$ ; and Model 4 was the same as Model 1 but with  $V_p$  calculated with Eqn 6, which introduces a PEP regeneration limitation. The *in vitro*  $V_{pmax}$  method calculates  $g_m$  by solving the system of two equations formed by the models of  $A$  and  $\Delta^{13}C$ . Therefore, once a solution is found,  $\phi$  values calculated with either Eqn 14 or 16 are identical. This is the case for Models 1, 2, and 4; however, in Model 3, which is constrained only by  $A$ ,  $\phi$  was obtained only with Eqn 14. All four modeling scenarios described above used the CA-limited calculations (Eqns 5–7).

At ambient  $pCO_2$ ,  $\phi$  was also calculated with a simplified equation derived from  $\Delta^{13}C$  assuming that  $C_{bs}$  is much larger than  $C_m$  and that hydration and assimilation fluxes are large ( $V_p/V_h \approx 0$ , and  $V_o \approx 0$ , where  $V_o$  is oxygenation rate):

$$\phi_2 = \frac{\Delta_{obs} (1-t) C_a - \bar{a} (C_a - C_i) - a_m C_i + C_m (a_m - \bar{b}_4)}{C_m (\bar{b}_3 - s)}, \quad \text{Eqn 19}$$

where  $\bar{b}_3$  and  $\bar{b}_4$  are (von Caemmerer *et al.*, 2014):

$$\bar{b}_3 = b_3' - \frac{eR_d}{A + R_d} + \frac{e0.5R_d}{A + 0.5R_d}, \quad \text{Eqn 20}$$

$$\bar{b}_4 = b_4' - \frac{e0.5R_d}{A + 0.5R_d}. \quad \text{Eqn 21}$$

Statistical analyses

Statistical analyses were performed using SAS v9.4 (SAS Institute Inc., Cary, NC, USA). Differences between CA-lim  $g_m$  and CA-sat  $g_m$  were investigated using  $t$ -tests ( $H_o$ : CA-lim  $g_m$ /CA-sat  $g_m$ =1). The effect of  $CO_2$  supply on CA-lim  $g_m$  was analysed using repeated measurements ANOVA. Data were log-transformed to meet normality criteria. In *Setaria* we used PROC MIXED with: *plant* as the repeated measurement;  $pCO_2$ , *temperature*, and their interaction as fixed effects; a covariance structure of compound symmetry; and we applied Kenward–Roger's approximation to correct the denominator degrees of freedom (Arnaud *et al.*, 2009). In *Zea*, we used PROC ANOVA with the statement REPEAT.

## Results

*A-C<sub>i</sub> curves and observed <sup>13</sup>C photosynthetic discrimination*

Under all leaf measurement temperatures ( $T_L$ ), the rate of net photosynthesis ( $A$ ) in *Setaria* increased with  $C_i$  as the  $pCO_2$  supplied increased from ~5 Pa to ambient air values (~35 Pa) and then leveled off (Fig. 1A). At all  $pCO_2$ , increasing  $T_L$  resulted in larger  $A$  (Fig. 1A). In *Zea*,  $A$  also increased with increasing  $C_i$  and reached a maximum at ambient air  $pCO_2$  before decreasing at higher  $pCO_2$  (Fig. 1B).

At ambient air  $pCO_2$  and 25 °C,  $\Delta^{13}_{obs}$  was larger in *Setaria* ( $4.5 \pm 0.1\%$ ) than in *Zea* ( $3.1 \pm 0.2\%$ ) (Fig. 1C, D). In *Zea*, the  $\Delta^{13}_{obs}$  was low at ambient air  $pCO_2$  and increased at lower or higher  $C_i$  (Fig. 1D). However, in *Setaria*,  $\Delta^{13}_{obs}$  remained constant with  $C_i$  when  $T_L$ =25 °C, but decreased as  $C_i$  increased both at 40 and 10 °C (Fig. 1C).

*Mesophyll conductance calculated assuming CA-saturated or CA-limited conditions*

For both species and at all temperatures, the ratio CA-lim  $g_m$ /CA-sat  $g_m \approx 1$  when  $pCO_2$  was above ambient (Fig. 2). As  $pCO_2$  decreased, CA-lim  $g_m$  became larger than CA-sat  $g_m$ ; the differences increased with temperature and were larger in *Zea* than in *Setaria*. In *Setaria*, CA-lim  $g_m$  and CA-sat  $g_m$  were significantly different ( $P < 0.05$ ) at all  $pCO_2$  at 40 °C, at all  $pCO_2$  except at ambient and the measurement just above



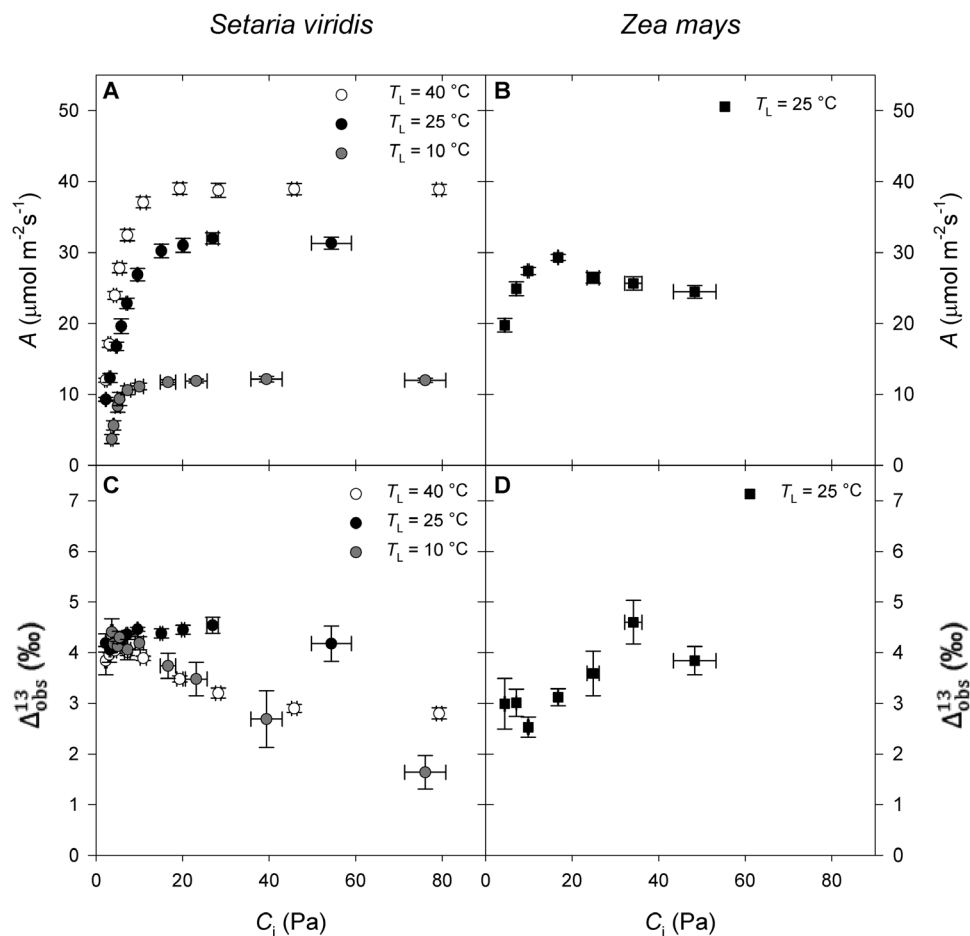


**Fig. 1.** Responses of (A, B) photosynthetic rate ( $A$ ) and (C, D) observed  $^{13}\text{C}$  photosynthetic discrimination ( $\Delta^{13}_{\text{obs}}$ ) to variation in the  $\text{CO}_2$  partial pressure inside the leaf ( $C_i$ ) in *Setaria viridis* (circles) and *Zea mays* (squares). In *Setaria*, three leaf temperatures ( $T_L$ ) were measured: 40, 25, and 10 °C, as indicated in the key. Measurements in *Zea* were at  $T_L=25$  °C. Values are means  $\pm$ SE;  $n=4$  in *Setaria* and  $n=3$  in *Zea*.

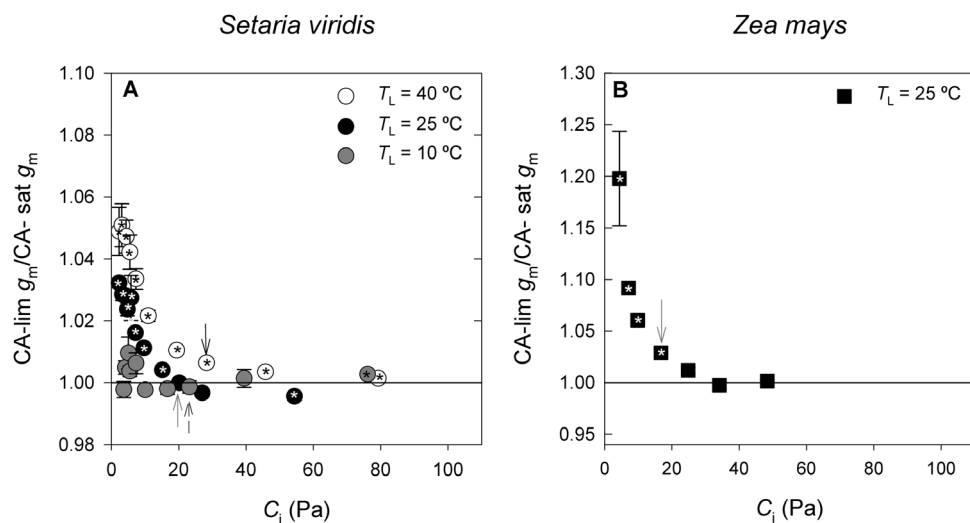


**Fig. 2.** The ratio of carbonic anhydrase-limited mesophyll conductance (CA-lim  $g_m$ ) to CA-saturated  $g_m$  (CA-sat  $g_m$ ) at different  $p\text{CO}_2$  inside the leaf ( $C_i$ ) in (A) *Setaria viridis* (circles) and (B) *Zea mays* (squares). *Setaria* was measured at three leaf temperatures ( $T_L$ ): 40, 25, and 10 °C, as indicated in the key. *Zea* was measured at  $T_L=25$  °C. Values are means  $\pm$ SE;  $n=4$  in *Setaria* and  $n=3$  in *Zea*. An asterisk inside a symbol indicates CA-lim  $g_m/\text{CA-sat } g_m \neq 1$  with  $P < 0.05$ . The arrows indicate the values at ambient  $p\text{CO}_2$  and at 40 °C (black arrow), 25 °C (grey arrow), and 10 °C (dashed arrow).

ambient at 25 °C, and at the largest  $p\text{CO}_2$  at 10 °C (Fig. 2A). In *Zea*, CA-lim  $g_m$  and CA-sat  $g_m$  were significantly different ( $P < 0.05$ ) at all  $p\text{CO}_2 \leq$  ambient air (Fig. 2B).

In *Setaria*, the under-estimation of  $g_m$  by ignoring the CA limitation was very small (maximum of 5%, CA-lim  $g_m/\text{CA-sat } g_m < 1.1$ ; Fig. 2A). However, in *Zea*, the CA-lim  $g_m$

calculated at the lowest  $p\text{CO}_2$  was  $20 \pm 8\%$  larger than CA-sat  $g_m$  at  $25^\circ\text{C}$ . Because CA limitation was relevant at low  $p\text{CO}_2$ , for subsequent analyses we use the CA-lim  $g_m$  values for all species, temperatures, and  $p\text{CO}_2$ .

#### $\text{CO}_2$ response of mesophyll conductance

The CA-lim  $g_m$  significantly increased as  $p\text{CO}_2$  decreased in *Setaria* at all temperatures ( $P < 0.0001$ ) and in *Zea* at  $25^\circ\text{C}$  ( $P < 0.0004$ ) (Fig. 3). At ambient  $p\text{CO}_2$  and  $25^\circ\text{C}$ , CA-lim  $g_m$  values (mean  $\pm$  SE) were  $2.00 \pm 0.10 \mu\text{mol m}^{-2} \text{s}^{-1} \text{Pa}^{-1}$  in *Setaria*, and  $2.43 \pm 0.13 \mu\text{mol m}^{-2} \text{s}^{-1} \text{Pa}^{-1}$  in *Zea*. At the lowest  $p\text{CO}_2$  measured ( $\sim 5\text{--}9 \text{ Pa}$ ) and  $25^\circ\text{C}$ , the CA-lim  $g_m$  increased to  $6.30 \pm 0.32$  and  $16.20 \pm 5.74 \mu\text{mol m}^{-2} \text{s}^{-1} \text{Pa}^{-1}$  in *Setaria* and *Zea*, respectively. Values for  $C_m$  across  $C_i$  can be found in Supplementary Fig. S1.

To compare the magnitude of the change in CA-lim  $g_m$  across species and temperatures, CA-lim  $g_m$  was normalized by dividing each value at a given temperature and  $p\text{CO}_2$  by CA-lim  $g_m$  at ambient  $p\text{CO}_2$  at that temperature (Fig. 3 D–F). At  $25^\circ\text{C}$ , the increase in CA-lim  $g_m$  with decreasing  $p\text{CO}_2$  was steeper in *Zea* than in *Setaria* (Fig. 3E). In *Setaria*, the

$g_m$   $p\text{CO}_2$  response was greatest at  $40^\circ\text{C}$  and there was little difference between the  $25$  and  $10^\circ\text{C}$  curves.

#### Limitations to photosynthesis

At elevated  $p\text{CO}_2$  assimilation rate was not limited by diffusion or substrate availability, as indicated by  $L_s$ ,  $L_m$ , and  $L_{CA} \approx 0\%$  for both species and all temperatures (Fig. 4). However, below ambient  $p\text{CO}_2$ , the diffusional limitation to  $A$  increased exponentially with decreasing  $p\text{CO}_2$ . The data in Fig. 4 show the different limitations as a function of the amount of substrate available:  $C_a$ ,  $C_i$ , and  $C_m$  for  $L_s$ ,  $L_m$ , and  $L_{CA}$ , respectively. In *Setaria*, diffusional limitations were lower at  $10^\circ\text{C}$  than at any other temperature. Comparing *Zea* and *Setaria* at  $25^\circ\text{C}$ , they had similar  $L_s$  but  $L_m$  was larger in *Setaria* than in *Zea*. For example, when  $C_a = 9 \text{ Pa}$ ,  $L_s = 23\%$  and  $19\%$  in *Setaria* and *Zea*, respectively. The corresponding  $C_i$  at this  $C_a$  was  $5 \text{ Pa}$  for both species, whereas  $L_m$  was almost double in *Setaria* ( $23\%$ ) compared to *Zea* ( $12\%$ ) (Fig. 4C, D). In both species,  $L_{CA}$  was small in comparison with  $L_s$  and  $L_m$ , and rapidly decreased below  $5\%$  as  $p\text{CO}_2$  increased.

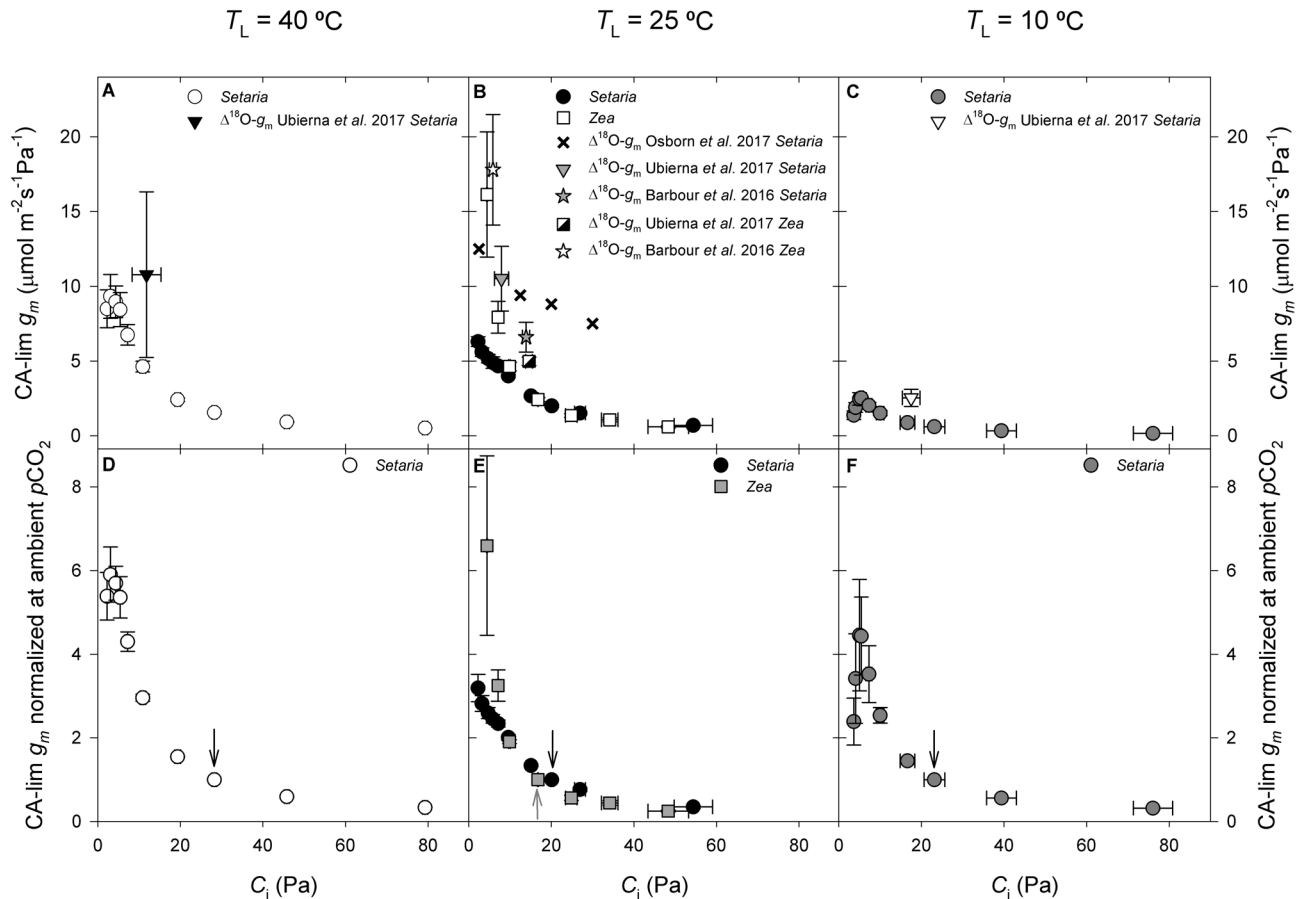


**Fig. 3.** The response of carbonic anhydrase-limited mesophyll conductance (CA-lim  $g_m$ ) to changes in  $p\text{CO}_2$  inside the leaf ( $C_i$ ) in (A, C) *Setaria viridis* (circles) and (B) *Zea mays* (white squares). *Setaria* was measured at three leaf temperatures, as indicated at the top of the figure. *Zea* was measured at  $T_L = 25^\circ\text{C}$ . For comparison, the available literature reports for  $\Delta^{18}\text{O}-g_m$  for different species and temperatures are included, as indicated in the keys: Ubierna et al. (2017) *Setaria* measured at  $T_L = 40^\circ\text{C}$ ,  $T_L = 25^\circ\text{C}$ , and  $T_L = 10^\circ\text{C}$ ; Osborn et al. (2017) *Setaria* measured at  $T_L = 25^\circ\text{C}$ ; Barbour et al. (2016) *Setaria* measured with block temperature of  $30^\circ\text{C}$ ; Ubierna et al. (2017) *Zea* measured at  $T_L = 25^\circ\text{C}$ ; Barbour et al. (2016) *Zea* measured with block temperature of  $30^\circ\text{C}$ . For all species and temperatures CA-lim  $g_m$  significantly varied with  $p\text{CO}_2$ . (D–F) The  $\text{CO}_2$  response of normalized  $g_m$ , calculated by dividing individual values by the  $g_m$  at ambient  $p\text{CO}_2$  at each temperature. Values are means  $\pm$  SE;  $n = 4$  in *Setaria*,  $n = 3$  in *Zea*. The arrows indicate the values at ambient  $p\text{CO}_2$ : black, *Setaria*; grey, *Zea*.

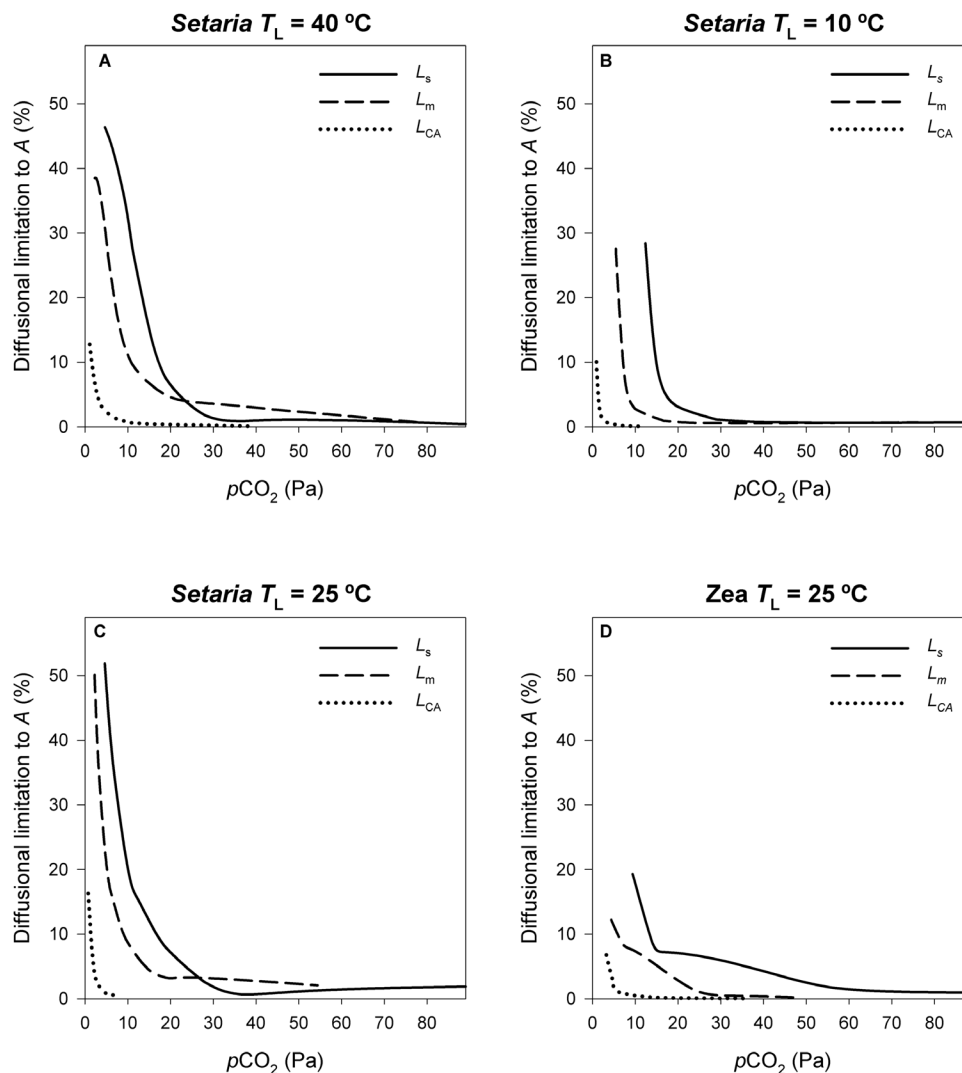


**Fig. 4.** Diffusional limitation to photosynthetic rate (A) imposed by stomatal resistance ( $L_s$ , Eqn 11, solid line), mesophyll resistance ( $L_m$ , Eqn 12, dashed line), and carbonic anhydrase ( $L_{CA}$ , Eqn 13, dotted line) as a function of the CO<sub>2</sub> supply ( $p\text{CO}_2$ ) available for each ( $C_a$ ,  $C_i$ , and  $C_m$  for  $L_s$ ,  $L_m$ , and  $L_{CA}$ , respectively). (A) *Setaria viridis* at  $T_L=40$  °C, (B) *Setaria viridis* at  $T_L=10$  °C, (C) *Setaria viridis* at  $T_L=25$  °C, and (D) *Zea mays* at  $T_L=25$  °C.

### Leakiness ( $\phi$ )

Values of  $\phi$  across  $p\text{CO}_2$  for *Setaria* and *Zea* at 25 °C calculated under different modeling assumptions are shown in Fig. 5. When  $g_m$  was finite and variable with  $p\text{CO}_2$  (Model 1),  $\phi$  increased from low to high  $p\text{CO}_2$ , with a range of 0.16–0.59 in *Zea* and 0.45–0.76 in *Setaria*. Assuming that  $g_m$  was infinite and  $V_{\text{pmax}}$  variable with  $p\text{CO}_2$  (Model 2) removed the  $p\text{CO}_2$  response of  $\phi$  and generally decreased  $\phi$  at all  $p\text{CO}_2$  in *Setaria*, but only at large  $p\text{CO}_2$  in *Zea*. Model 3 resulted in nearly identical  $\phi$  to Model 2 using the same finite  $g_m$  as Model 1 but with the solution constrained by only the photosynthesis model. However, this scenario failed to predict  $\Delta^{13}_{\text{obs}}$  (see Supplementary Fig. S2). Imposing a PEP regeneration rate ( $V_{\text{pr}}$ ) limitation of 64 and 59  $\mu\text{mol m}^{-2} \text{s}^{-1}$  in *Setaria* and *Zea*, respectively (Model 4), decreased  $\phi$  compared to the results with Model 1 in *Setaria* but resulted in no change in *Zea*. Interestingly, at  $p\text{CO}_2 \leq$  ambient air, values for  $\phi$  were similar across models in *Zea*, but they differed in *Setaria*. The values of  $V_{\text{pmax}}$ ,  $V_{\text{cmax}}$ ,  $V_{\text{p}}$ ,  $V_{\text{c}}$ ,  $C_{\text{bs}}$ , and  $g_{\text{bs}}$  used in these four models are reported in Supplementary Fig. S2.

For comparison we also present  $\phi$  at ambient  $p\text{CO}_2$  calculated with the simplified Eqn 19 and assuming either  $g_m$  finite or infinite. For both species,  $\phi$  calculated with Eqn 19 was not different to values obtained with the complete Eqn 16 when  $g_m$  was finite (compare black lines and black symbols in Fig. 5) and when  $g_m$  was infinite (compare grey dashed line and clear symbols).

## Discussion

### Calculation of mesophyll conductance and model parameterization

Mesophyll conductance ( $g_m$ ) was derived with the *in vitro*  $V_{\text{pmax}}$  method (Ubierna *et al.*, 2017). Estimations of  $g_m$  with this method were similar to  $\Delta^{18}\text{O}-g_m$  across temperatures (Ubierna *et al.*, 2017) and across  $p\text{CO}_2$  (Kolbe and Cousins, 2018). Potential errors in  $g_m$  originating from inaccurate model parameterization of the *in vitro*  $V_{\text{pmax}}$  method were tested with a sensitivity analysis using *Setaria* data at three

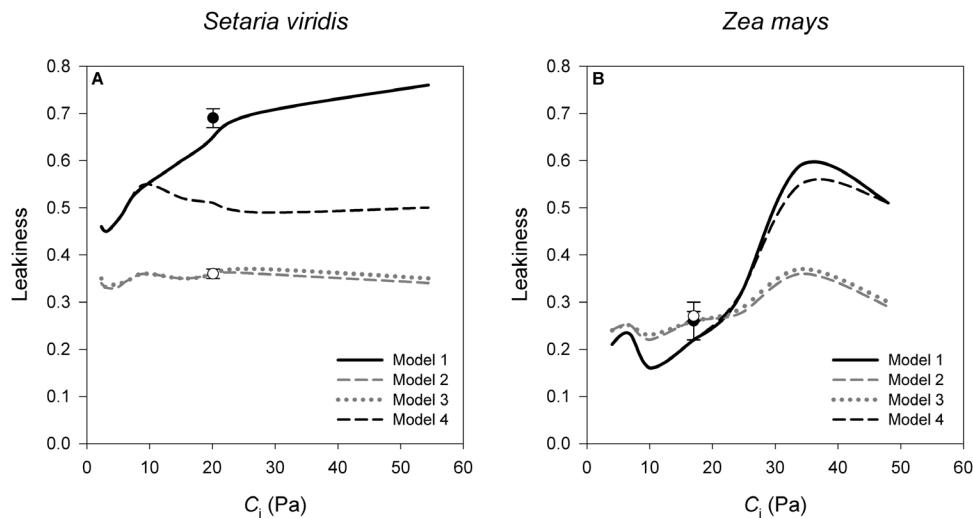


**Fig. 5.** Effect of different parameterizations of models of photosynthesis in the calculation of leakiness ( $\phi$ ) in (A) *Setaria viridis* and (B) *Zea mays* at 25 °C and over a range of  $p\text{CO}_2$  inside the leaf intercellular spaces ( $C_i$ ). Model 1 (solid black line) uses *in vitro*  $V_{p\text{max}}$  and  $g_m$  finite and equal to the values presented in Fig. 3; Model 2 (dashed grey line) uses *in vivo*  $V_{p\text{max}}$  (which is variable with  $p\text{CO}_2$ , see Supplementary Fig. S2) and  $g_m$  infinite; Model 3 (dotted grey line) uses the same as Model 1 but the solution was only constrained by  $A$  and not  $\Delta^{13}\text{C}$ ; Model 4 (dashed black line) uses the same as Model 1 but introducing  $V_{pr}$  (= 64 and 59  $\mu\text{mol m}^{-2} \text{s}^{-1}$  in *Setaria* and *Zea*, respectively) in the calculation of  $V_p$  (Eqn 6). The rest of the variables included in these models were calculated as explained in the Methods section: values for some of them can be found in Supplementary Fig. S2. In Models 1, 2, and 4,  $\phi$  was calculated with Eqns 14 or 16 (same result) and in Model 3,  $\phi$  was calculated with Eqn 14. The symbols indicate the value of  $\phi$  at ambient air  $p\text{CO}_2$  calculated with the simplified Eqn 19 assuming either  $g_m$  finite (solid symbols) or infinite (clear symbols). Values are means  $\pm$  SE;  $n=4$  in *Setaria*,  $n=3$  in *Zea*.

temperatures and across  $p\text{CO}_2$  (see Supplementary Fig. S3). Halving *in vitro*  $V_{p\text{max}}$  increased  $g_m$  by <20% at large  $p\text{CO}_2$  and almost doubled it at low  $p\text{CO}_2$  and high temperature. Alternatively, doubling *in vitro*  $V_{p\text{max}}$  decreased  $g_m$  by <15% at all  $p\text{CO}_2$  and temperatures (Supplementary Fig. S3J–L). This demonstrates that uncertainties in *in vitro*  $V_{p\text{max}}$  affect absolute values of  $g_m$ , but not the trend of increasing  $g_m$  with decreasing  $p\text{CO}_2$ . The sensitivity analysis also demonstrated that variations up to  $\pm 50\%$  in  $K_p$ ,  $K_C$ , or  $K_{CA}$  resulted in negligible (when  $p\text{CO}_2 \geq \text{ambient}$ ) or small (at low  $p\text{CO}_2$ ) errors in  $g_m$  calculations at any temperature (Supplementary Fig. S3A–I) and did not affect the observed trend of  $g_m$  with  $p\text{CO}_2$ .

In  $C_3$  plants, it has been suggested that large  $g_m$  values reported for low  $p\text{CO}_2$  might be an artifact of uncertainties in parameters such as  $R_d$ ,  $\Gamma^*$ , and  $b_3'$  (Gu and Sun, 2014). The simulations with different values for  $R_d$  (see Supplementary Fig. S4A, B) or  $b_3'$  (Supplementary Fig. S4C, D) resulted in variations in  $g_m$  of <6% and did not affect the trend of increasing  $g_m$  with decreasing  $p\text{CO}_2$ . Ubierna et al. (2017) demonstrated that  $g_m$  is largely independent of values of  $g_{bs}$  or  $V_{c\text{max}}$  and this is also illustrated in Supplementary Fig. S2.

#### CA-limited versus CA-saturated models to estimate $g_m$

The substrate for the initial carboxylation by PEPC is  $\text{HCO}_3^-$  and not  $\text{CO}_2$ . However,  $V_p$  is often calculated in terms of  $\text{CO}_2$ , because the hydration of  $\text{CO}_2$  ( $V_h$ ) generally happens very fast when catalysed by CA (Stryer, 1988). We refer to this case as the CA-saturated model. In contrast, the CA-limited model calculates  $V_p$  as a function of  $\text{HCO}_3^-$ . The value of  $\text{HCO}_3^-$  is calculated with  $C_m$ ,  $V_h$ ,  $V_{p\text{max}}$ , and a series of rate constants (see Ubierna et al., 2017, for details). Producing the same  $V_p$  with the CA-limited and the CA-saturated

calculations requires larger  $C_m$  for the former than the latter, and the difference could potentially be large if  $V_h$  is low. Subsequently, neglecting the hydration step, as in the CA-saturated calculations, can result in under-estimation of  $C_m$  and  $g_m$ . The terminology CA-saturated or -limited refers to the modeling of  $V_p$  and how this affects the calculated  $C_m$  value, but it does not imply different roles of CA in the photosynthetic process. Ubierna et al. (2017) found no difference between CA-sat  $g_m$  and CA-lim  $g_m$  at ambient  $p\text{CO}_2$ ; however, the aim here is to compare these calculations for a range of  $p\text{CO}_2$ .

In both species and at all temperatures, the difference between CA-sat  $g_m$  and CA-lim  $g_m$  was negligible for  $p\text{CO}_2 > \text{ambient}$  (Fig. 2). However, as  $p\text{CO}_2$  decreased, CA-lim  $g_m$  became larger than CA-sat  $g_m$ , especially at high temperatures and in *Zea*. In this species ignoring the hydration step resulted in under-estimating  $g_m$  by as much as 20%, whereas in *Setaria* the under-estimation was <5%.

The larger differences at high temperatures can be explained by the temperature response of  $K_{CA}$ , which increases from 10 to 30 °C but plateaus above that (Boyd et al., 2015). Species differences can be explained by different  $K_{CA}$  values and  $\text{CO}_2$  availability to CA. Firstly,  $K_{CA}$  in *Setaria* (124  $\mu\text{mol m}^{-2} \text{s}^{-1} \text{Pa}^{-1}$ ) was double the value for *Zea* (65.5  $\mu\text{mol m}^{-2} \text{s}^{-1} \text{Pa}^{-1}$ ). Below ambient  $p\text{CO}_2$ , *Setaria* and *Zea* had similar  $A$ ,  $g_s$ , and  $C_i$ . Sustaining similar  $A$  in these two species requires larger  $C_m$  in *Zea* than in *Setaria* because of the lower *in vitro*  $V_{p\text{max}}$  value in the former (184  $\mu\text{mol m}^{-2} \text{s}^{-1}$ ) versus the latter (450  $\mu\text{mol m}^{-2} \text{s}^{-1}$ ). Therefore, in *Zea* the lower  $K_{CA}$  and *in vitro*  $V_{p\text{max}}$  was counterbalanced by increased  $\text{CO}_2$  availability to CA through higher  $g_m$ . Osborn et al. (2017) also suggested large  $g_m$  as a mechanism to increase  $\text{CO}_2$  assimilation rate at low  $p\text{CO}_2$ .



At low  $p\text{CO}_2$  or in species with low  $K_{\text{CA}}$ , ignoring the hydration step results in under-estimation of  $g_m$ . However, the error is insignificant at  $p\text{CO}_2$  above ambient or in species with large  $K_{\text{CA}}$ , such as *Setaria*. The hydration step should be included for accurate determination of  $g_m$  at low  $p\text{CO}_2$  in species with low  $K_{\text{CA}}$  and/or high  $A$ , such as C<sub>4</sub> grasses (Cousins *et al.*, 2008), especially at high temperatures.

#### Values for CA-lim $g_m$ and variation with $p\text{CO}_2$

Across  $p\text{CO}_2$  and temperatures, CA-lim  $g_m$  ranged from  $0.6 \pm 0.1$  to  $9.3 \pm 1.5 \mu\text{mol m}^{-2} \text{s}^{-1} \text{Pa}^{-1}$  in *Setaria*, and  $0.6 \pm 0.1$  to  $16.2 \pm 5.7 \mu\text{mol m}^{-2} \text{s}^{-1} \text{Pa}^{-1}$  in *Zea* (Fig. 3). In *Zea*, photosynthetic rate declined above ambient  $p\text{CO}_2$ , indicating deactivation at low  $C_i$  that did not fully recover when  $p\text{CO}_2$  supply was returned to ambient levels (Fig. 1B). This could have introduced some bias in the CA-lim  $g_m$  values calculated at high  $p\text{CO}_2$ . Nevertheless, the CA-lim  $g_m$  values were used at  $p\text{CO}_2 \leq$  ambient, because above ambient, photosynthesis was not restricted by diffusional limitations (Fig. 4).

To validate CA-lim  $g_m$  values, they were compared with literature reports for the same species obtained with the alternative  $\Delta^{18}\text{O}$  method (Barbour *et al.*, 2016; Osborn *et al.*, 2017; Ubierna *et al.*, 2017; Fig. 3). In *Zea*, there was a good agreement between  $\Delta^{18}\text{O}$ - $g_m$  (Barbour *et al.*, 2016; Ubierna *et al.*, 2017) and CA-lim  $g_m$  (Fig. 3B). A recent study in *Zea* by Kolbe and Cousins (2018) also found agreement between  $\Delta^{18}\text{O}$ - $g_m$  and *in vitro*  $V_{\text{pmax}} g_m$  across a range of  $p\text{CO}_2$ , although both estimations of  $g_m$  deviated at very low  $p\text{CO}_2$ . In *Setaria*,  $\Delta^{18}\text{O}$ - $g_m$  (Barbour *et al.*, 2016; Osborn *et al.*, 2017; Ubierna *et al.*, 2017) was larger than our CA-lim  $g_m$  results (Fig. 3A–C). This discrepancy could have originated if *in vitro*  $V_{\text{pmax}}$  was over-estimated, and more studies exploring  $g_m$  variation and assessing the impacts of the method are needed.

In *Zea* at 25 °C and in *Setaria* at three temperatures, the CA lim- $g_m$  increased with short-term exposure to decreasing  $p\text{CO}_2$ . Increasing  $g_m$  with decreasing  $p\text{CO}_2$  has also been observed in C<sub>3</sub> species (Bongi and Loreto, 1989; Loreto *et al.*, 1992; Flexas *et al.*, 2007, 2008; Hassiotou *et al.*, 2009; Bunce, 2010; Douthe *et al.*, 2011; Tazoe *et al.*, 2011), although there are also a few studies that have concluded there is no change (Loreto *et al.*, 1992; Tazoe *et al.*, 2009). There are only two studies that have presented C<sub>4</sub>- $g_m$  across  $p\text{CO}_2$ . In Osborn *et al.* (2017),  $\Delta^{18}\text{O}$ - $g_m$  values for *Setaria* increased with decreasing  $p\text{CO}_2$  but the trend was not significant. In *Zea*, Kolbe and Cousins (2018) found a significant increase in  $\Delta^{18}\text{O}$ - $g_m$  with decreasing  $p\text{CO}_2$ .

The initial slope of an  $A$ - $C_i$  curve can be modified with either  $C_m$  ( $g_m$ ) or  $V_{\text{pmax}}$  (see Supplementary Fig. S5). Therefore, there may be a value for  $V_{\text{pmax}}$  that would cancel out the trend in CA-lim  $g_m$ . However, this is not the case if  $V_{\text{pmax}}$  is independent of  $p\text{CO}_2$ , and cancelling the observed trend in CA-lim  $g_m$  would require  $V_{\text{pmax}}$  to decrease with increasing  $p\text{CO}_2$  (Supplementary Fig. S6). There is evidence showing that CO<sub>2</sub> levels affect the phosphorylation state of PEPC and PEPC, and therefore variation of *in vitro*  $V_{\text{pmax}}$  across  $p\text{CO}_2$  could be expected (Bailey *et al.*, 2007). However, the CO<sub>2</sub> response of photosynthetic rate was found to be no

different between wild-type and transgenic plants with low PEPC phosphorylation (Furumoto *et al.*, 2007). Much of the post-translational modifications that presumably lower  $V_{\text{pmax}}$  would probably occur when CO<sub>2</sub> is saturating and some other factor limits C<sub>4</sub> photosynthesis. At ambient  $p\text{CO}_2$  and below it is generally thought, although not known, that PEPC is operating at  $V_{\text{pmax}}$ . The fact that  $\Delta^{18}\text{O}$ - $g_m$  data have demonstrated a similar trend of increasing  $g_m$  with decreasing  $p\text{CO}_2$  (Kolbe and Cousins, 2018) points to a constant  $V_{\text{pmax}}$  value. Nevertheless, if fast *in vivo* regulation of  $V_{\text{pmax}}$  occurs it could alter values and trends in  $g_m$ . In reality, there might be a combination of both fluctuations in  $g_m$  and  $V_{\text{pmax}}$  in response to short-term variation in  $p\text{CO}_2$ . Future work should investigate *in vivo* regulation of  $V_{\text{pmax}}$  and its impact on  $g_m$  calculations.

#### Limitation to photosynthesis at low $p\text{CO}_2$

C<sub>4</sub> photosynthesis saturates at ambient  $p\text{CO}_2$  and  $A$  was not limited by diffusion, as indicated by  $L_s$ ,  $L_m$ , and  $L_{\text{CA}} \approx 0\%$  for both species and all temperatures (Fig. 4). However, below ambient air  $p\text{CO}_2$ , diffusional limitations constrained CO<sub>2</sub> assimilation and increased exponentially with decreasing  $p\text{CO}_2$ . As shown in Fig. 1 and Supplementary Fig. S5, in both species the CO<sub>2</sub> responsive part of the  $A$ - $C_i$  curve corresponded to  $C_i$  below  $\sim 10$  Pa. This raises the question of whether C<sub>4</sub> plants operate below this threshold. In laboratory experiments, high irradiance and N fertilization shifted the operational  $C_i$  down to the CO<sub>2</sub> responsive part of the  $A$ - $C_i$  curve (Ghannoum *et al.*, 1997; Ghannoum and Conroy, 1998). Additionally, moderate water stress decreased  $C_i$  in several C<sub>4</sub> species, although under severe drought declines in  $A$  precluded  $C_i$  from getting very low (Ghannoum, 2009, and references herein). Under ambient air  $p\text{CO}_2$ ,  $C_i < 11$  Pa were reported for *Zea* grown in FACE-type experiments (Leakey *et al.*, 2004; Markelz *et al.*, 2011), and *Sorghum bicolor* grown in an open field reached  $C_i/C_a = 0.2$  after two consecutive water-stress cycles (Steduto *et al.*, 1997). Therefore, under certain growth conditions, CO<sub>2</sub> availability may limit C<sub>4</sub> photosynthesis.

Interestingly, *Setaria* and *Zea* displayed different behavior at low  $p\text{CO}_2$ . At low  $p\text{CO}_2$ , *Zea* was more efficient because it achieved high  $A$  despite lower  $V_{\text{pmax}}$  and  $K_{\text{CA}}$  by decreasing diffusional limitations and sustaining greater  $C_m$  with high  $g_m$ . The high  $g_m$  at low  $p\text{CO}_2$  could increase or maintain photosynthesis at low  $C_i$  and could improve photosynthetic rates under situations that result in low CO<sub>2</sub> availability, such as drought.

In both species, the conversion of CO<sub>2</sub> into bicarbonate as catalysed by CA was fast enough that the hydration rate only limited  $A$  at low  $p\text{CO}_2$  ( $L_{\text{CA}} = 6$ – $16\%$  for  $C_m < 4$  Pa, Fig. 4). Such low  $C_m$  is unlikely to occur, even under drought conditions. At these very low  $p\text{CO}_2$ , the hydration rate ( $V_h$ ) was comparable to rates in CA-depleted transgenic plants (Supplementary Fig. S7). For example, in *Setaria* at 25 °C,  $V_h$  decreased from  $581 \mu\text{mol m}^{-2} \text{s}^{-1}$  at ambient  $p\text{CO}_2$  to  $100 \mu\text{mol m}^{-2} \text{s}^{-1}$  at the lowest  $p\text{CO}_2$  measured. Using values from Osborn *et al.* (2017) at 25 °C and ambient  $p\text{CO}_2$  to calculate  $V_h$  as  $C_m \times K_{\text{CA}}$  resulted in 1215 and  $142 \mu\text{mol m}^{-2} \text{s}^{-1}$

for the wild type and CA-depleted transgenic, respectively. Osborn et al. (2017) concluded that in *Setaria* at low  $p\text{CO}_2$ ,  $g_m$  posed a greater limitation than CA activity. Our study confirms that  $g_m$  is a major determinant of photosynthetic capacity at low  $p\text{CO}_2$  and CA further constrains assimilation rates only at very low  $p\text{CO}_2$ . However, the CA limitation at low  $p\text{CO}_2$  will be exacerbated at higher temperatures as the hydration rate is less able to keep up with the increase in PEPC activity (Boyd et al., 2015).

### Leakiness ( $\phi$ )

Leakiness is often estimated from comparing models and measurements of  $\Delta^{13}\text{C}$  assuming  $g_m$  is infinite (Pengelly et al., 2010; Ubierna et al., 2011, 2013) or large (Kromdijk et al., 2010). Values of  $\phi$  vary by as much as 0.04–0.9 (for a compilation of values and review of methods see Kromdijk et al., 2014), although for most species under most conditions  $\phi=0.2$ –0.3 (Cousins et al., 2006; Kromdijk et al., 2010; Pengelly et al., 2010; Ubierna et al., 2013; Bellasio and Griffiths, 2014).

In our study, considering  $g_m$  to be finite had a different effect on the calculation of  $\phi$  for *Setaria* and *Zea*. At ambient air  $p\text{CO}_2$  and 25 °C, both *Setaria* and *Zea* had similar  $g_m$  (2.00 and 2.43  $\mu\text{mol m}^{-2} \text{s}^{-1} \text{Pa}^{-1}$ , respectively). However, while  $\phi$  in *Zea* was the same whether  $g_m$  was finite or infinite, in *Setaria*, accounting for a finite  $g_m$  doubled  $\phi$  (Fig. 5, compare Models 1 and 2). This high  $\phi$  in *Setaria* was driven by constraints imposed by the  $\Delta^{13}\text{C}$  model rather than the photosynthesis model. This is illustrated by the comparison of Models 2 and 3 (Fig. 5). Both models predicted the same  $A$  and  $\phi$ , but Model 2 used  $g_m$  finite (and *in vitro*  $V_{p\text{max}}$ ) and Model 3 assumed  $g_m$  infinite (and *in vivo*  $V_{p\text{max}}$ ). However, Model 3 failed to predict  $\Delta^{13}_{\text{obs}}$  (see Supplementary Fig. S2). Forcing the solution to satisfy both models of  $A$  and  $\Delta^{13}_{\text{obs}}$  resulted in increases in  $\phi$  in *Setaria*, but not in *Zea*.

This can be explained through the relationship between  $\Delta^{13}\text{C}$  and  $C_m/C_a$ , which is illustrated in Fig. 6 for different values of  $\phi$ . Increasing  $C_m/C_a$  results in either increased or decreased  $\Delta^{13}\text{C}$  depending on whether  $\phi$  is low ( $\leq 0.3$ ) or high (Henderson et al., 1992; von Caemmerer et al., 2014). When  $\Delta^{13}_{\text{obs}} > a_s + (a_m - a_s)(C_i/C_a)$  ( $= 4.4 - 2.6 C_i/C_a \approx 2.9\text{‰}$  in our data set at 25 °C and ambient  $p\text{CO}_2$ ) increasing  $C_m/C_a$  results in decreased  $\phi$ ; meanwhile the opposite is true when  $\Delta^{13}_{\text{obs}} < 4.4 - 2.6 C_i/C_a$ . The value  $a_s + (a_m - a_s)(C_i/C_a)$  represents the intercept of the line  $\Delta^{13}\text{C}$  versus  $C_m/C_a$  when  $C_{\text{bs}}$  and boundary layer conductance are large and ternary effects are ignored. At ambient air  $p\text{CO}_2$  and 25 °C,  $\Delta^{13}_{\text{obs}} = 3.1\text{‰}$  in *Zea*. Therefore, varying  $C_m/C_a$  resulted in minimal changes in  $\phi$  (compare black triangle and circle in Fig. 6). However, in *Setaria*,  $\Delta^{13}_{\text{obs}} = 4.5\text{‰}$  and therefore low  $C_m/C_a$  translated into large  $\phi$  (compare grey triangle and circle in Fig. 6). The photosynthesis model demonstrated that this increase in  $\phi$  was achieved by increased  $V_p$  and  $g_{\text{bs}}$  (see Supplementary Fig. S2).

It is questionable that *Setaria* operates with  $\phi=0.7$ , and it is seemingly unreasonable that it does. Because  $\Delta^{13}\text{C}$  is mostly determined by  $C_m/C_a$  and  $\phi$ , low  $C_m/C_a$  forces the increase in  $\phi$ . But are there any other parameters in the discrimination

equation that could be manipulated in order to predict large  $\Delta^{13}\text{C}$  with low  $C_m/C_a$  without large  $\phi$ ? Calculations of  $\phi$  with the complete (Eqn 16) and simplified (Eqn 19) models suggest that, at least at ambient  $p\text{CO}_2$ , this was not the case. The simplified calculation of  $\phi$  produced values similar to the complete model, suggesting that at ambient air  $p\text{CO}_2$  or above, modifying parameters such as  $C_{\text{bs}}$ ,  $b_3$ , or  $b_4$  within their current definition did not result in large changes in  $\Delta^{13}\text{C}$ .

In addition to the possible post-translational regulation of  $V_{p\text{max}}$ , PEP regeneration ( $V_{\text{pr}}$ ) may also influence  $V_p$  (Eqn 6) and estimates of  $\phi$ . In our calculations,  $V_{\text{pr}}=64 \mu\text{mol m}^{-2} \text{s}^{-1}$  decreased  $\phi$  in *Setaria* by 0.3 and resulted in slightly larger  $g_m$  values at high  $p\text{CO}_2$  but no change at low  $p\text{CO}_2$  (compare Models 1 and 4 in Fig. 5 and Supplementary Fig. S2). In fact, at low  $p\text{CO}_2$  it is expected that  $V_{\text{pr}}$  would not limit  $V_p$  and would have no effect on estimates of  $g_m$  or  $\phi$  under these conditions. Changes in  $\phi$  in response to  $p\text{CO}_2$  or other conditions are possible if  $V_{\text{pr}}$  is allowed to vary, although at present  $V_{\text{pr}}$  variation across species, temperatures, or  $p\text{CO}_2$  is unknown. The  $V_{\text{pr}}$  values that would be needed to remove the observed trend in  $g_m$  with  $p\text{CO}_2$  are shown in Supplementary Fig. S8. Introducing a value for  $V_{\text{pr}}$  implies decoupling  $V_p$  from  $C_m$  ( $g_m$ ). In other words, the required  $V_p$  value to support the measured  $A$  could be achieved by choosing the adequate  $V_{\text{pr}}$  rather than by varying  $C_m$ . This would also further complicate estimations of  $\phi$  from  $\Delta^{13}\text{C}$  as  $V_{\text{pr}}$  is not often measured and is not incorporated into the  $\Delta^{13}\text{C}$  models.

Our calculations assume that theoretical models of photosynthesis and discrimination represent the actual photosynthetic

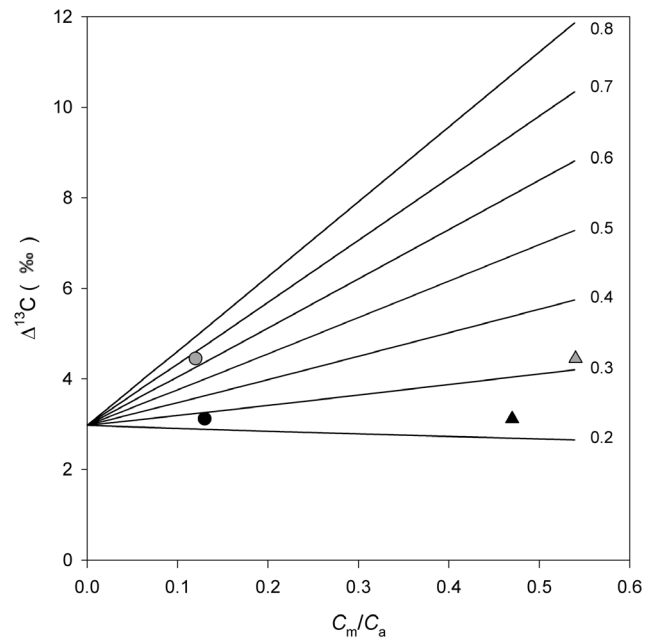


**Fig. 6.**  $\Delta^{13}\text{C}$  (Eqn 9) as a function of  $C_m/C_a$  for different  $\phi$  values (indicated by the numbers at the end of each line). For calculations we used values of 37, 36, 20, and 1364 Pa for  $C_a$ ,  $C_L$ ,  $C_i$ , and  $C_{\text{bs}}$ , respectively;  $t=0.0058$ ,  $b_4=-4.49\text{‰}$ , and  $b_3=29.87\text{‰}$ . These values correspond to the mean values measured or calculated in *Setaria* at 25 °C and ambient  $p\text{CO}_2$ . Black symbols represent data for *Zea* and grey symbols for *Setaria*. For both species,  $\phi$  was calculated assuming either  $g_m$  infinite (triangles) or  $g_m=2.00$  and 2.43  $\mu\text{mol m}^{-2} \text{s}^{-1} \text{Pa}^{-1}$  in *Setaria* and *Zea*, respectively (circles).

process; any inaccuracy in the models will introduce error in the calculated  $g_m$ . We have evaluated one common modelling simplification, the effect of CA limitation, and also the impact of uncertainty on input parameters. Additionally, we have used two contrasting species to illustrate the sensitivity of  $\phi$  to  $g_m$ . Although a complete analysis of  $\phi$  is beyond the scope of this work, this should be undertaken in future studies together with investigations on PEP regeneration limitations. Other future foci for research include: investigating *in vivo* and *in vitro*  $V_{\text{pmax}}$  values and variation across species and environmental conditions; and compiling leaf structure, CA, aquaporins, or other data that could reveal potential mechanisms behind observed  $g_m$  patterns.

## Supplementary data

Supplementary data are available at *JXB* online.

Methods S1. Model of <sup>13</sup>C discrimination in C<sub>4</sub> species.

Table S1. Gas exchange values for C<sub>i</sub> and A, and calculated values for C<sub>m</sub> and CA-lim  $g_m$  in *Setaria viridis* and *Zea mays* at 25 °C and variable CO<sub>2</sub> supply.

Fig. S1. C<sub>m</sub> across C<sub>i</sub> in *Setaria viridis* at three temperatures, and in *Zea mays* at 25 °C.

Fig. S2. Description of the models used to evaluate the effect of  $g_m$  in calculations of  $\phi$ .

Fig. S3. Sensitivity of calculations of CA-lim  $g_m$  in *Setaria viridis* to uncertainty in input parameters.

Fig. S4. Impact of R<sub>d</sub> and b<sub>3</sub> in the calculation of CA-lim  $g_m$  in *Setaria viridis* at 25 °C.

Fig. S5. Measured versus modeled response of A to C<sub>i</sub> at 25 °C in *Setaria viridis* and *Zea mays* for different values of V<sub>pmax</sub> and  $g_m$ .

Fig. S6. Values for *in vivo* V<sub>pmax</sub> across C<sub>i</sub> in *Setaria viridis* calculated when CA-lim  $g_m$  is constant with pCO<sub>2</sub>.

Fig. S7. V<sub>h</sub> across C<sub>i</sub> in *Setaria viridis* at three temperatures.

Fig. S8. Values for V<sub>pr</sub> across C<sub>i</sub> in *Setaria viridis* calculated when CA-lim  $g_m$  is constant with pCO<sub>2</sub>.

## Acknowledgments

This research was supported by the Division of Chemical Sciences, Geosciences and Biosciences, Office of Basic Energy Sciences, Photosynthetic Systems through DE-SC0001685 and with instrumentation from an NSF Major Research Instrumentation grant #0923562. We thank an anonymous reviewer for valuable comments that improved this manuscript.

## References

- Arnau J, Bono R, Vallejo G.** 2009. Analyzing small samples of repeated measures data with the mixed-model adjusted *F* test. *Communications in Statistics - Simulation and Computation* **38**, 1083–1103.
- Bailey KJ, Gray JE, Walker RP, Leegood RC.** 2007. Coordinate regulation of phosphoenolpyruvate carboxylase and phosphoenolpyruvate carboxykinase by light and CO<sub>2</sub> during C<sub>4</sub> photosynthesis. *Plant Physiology* **144**, 479–486.
- Barbour MM, Evans JR, Simonin KA, von Caemmerer S.** 2016. Online CO<sub>2</sub> and H<sub>2</sub>O oxygen isotope fractionation allows estimation of mesophyll conductance in C<sub>4</sub> plants, and reveals that mesophyll conductance decreases as leaves age in both C<sub>4</sub> and C<sub>3</sub> plants. *New Phytologist* **210**, 875–889.
- Bellasio C, Griffiths H.** 2014. Acclimation to low light by C<sub>4</sub> maize: implications for bundle sheath leakiness. *Plant, Cell & Environment* **37**, 1046–1058.
- Bongi G, Loreto F.** 1989. Gas-exchange properties of salt-stressed olive (*Olea europaea* L.) leaves. *Plant Physiology* **90**, 1408–1416.
- Boyd RA, Gandin A, Cousins AB.** 2015. Temperature responses of C<sub>4</sub> photosynthesis: biochemical analysis of Rubisco, phosphoenolpyruvate carboxylase, and carbonic anhydrase in *Setaria viridis*. *Plant Physiology* **169**, 1850–1861.
- Bunce JA.** 2010. Variable responses of mesophyll conductance to substomatal carbon dioxide concentration in common bean and soybean. *Photosynthetica* **48**, 507–512.
- Cousins AB, Badger MR, von Caemmerer S.** 2006. Carbonic anhydrase and its influence on carbon isotope discrimination during C<sub>4</sub> photosynthesis. Insights from antisense RNA in *Flaveria bidentis*. *Plant Physiology* **141**, 232–242.
- Cousins AB, Badger MR, von Caemmerer S.** 2008. C<sub>4</sub> photosynthetic isotope exchange in NAD-ME- and NADP-ME-type grasses. *Journal of Experimental Botany* **59**, 1695–1703.
- Doutte C, Dreyer E, Epron D, Warren CR.** 2011. Mesophyll conductance to CO<sub>2</sub>, assessed from online TDL-AS records of <sup>13</sup>CO<sub>2</sub> discrimination, displays small but significant short-term responses to CO<sub>2</sub> and irradiance in *Eucalyptus* seedlings. *Journal of Experimental Botany* **62**, 5335–5346.
- Edwards GE, Walker DA.** 1983. C<sub>3</sub>, C<sub>4</sub>: Mechanisms, and cellular and environmental regulation of photosynthesis. Oxford, UK: Blackwell Scientific Publications.
- Evans JR.** 1983. Nitrogen and photosynthesis in the flag leaf of wheat (*Triticum aestivum* L.). *Plant Physiology* **72**, 297–302.
- Evans JR, Sharkey TD, Berry JA, Farquhar GD.** 1986. Carbon isotope discrimination measured concurrently with gas exchange to investigate CO<sub>2</sub> diffusion in leaves of higher plants. *Australian Journal of Plant Physiology* **13**, 281–292.
- Evans JR, Terashima I.** 1988. Photosynthetic characteristics of spinach leaves grown with different nitrogen treatments. *Plant and Cell Physiology* **29**, 157–165.
- Evans JR, von Caemmerer S.** 1996. Carbon dioxide diffusion inside leaves. *Plant Physiology* **110**, 339–346.
- Farquhar GD.** 1983. On the nature of carbon isotope discrimination in C<sub>4</sub> species. *Australian Journal of Plant Physiology* **10**, 205–226.
- Farquhar GD, Cernusak LA.** 2012. Ternary effects on the gas exchange of isotopologues of carbon dioxide. *Plant, Cell & Environment* **35**, 1221–1231.
- Farquhar GD, Sharkey TD.** 1982. Stomatal conductance and photosynthesis. *Annual Review of Plant Physiology* **33**, 317–345.
- Flexas J, Diaz-Espejo A, Galmés J, Kaldenhoff R, Medrano H, Ribas-Carbo M.** 2007. Rapid variations of mesophyll conductance in response to changes in CO<sub>2</sub> concentration around leaves. *Plant, Cell & Environment* **30**, 1284–1298.
- Flexas J, Ribas-Carbo M, Diaz-Espejo A, Galmés J, Medrano H.** 2008. Mesophyll conductance to CO<sub>2</sub>: current knowledge and future prospects. *Plant, Cell & Environment* **31**, 602–621.
- Furumoto T, Izui K, Quinn V, Furbank RT, von Caemmerer S.** 2007. Phosphorylation of phosphoenolpyruvate carboxylase is not essential for high photosynthetic rates in the C<sub>4</sub> species *Flaveria bidentis*. *Plant Physiology* **144**, 1936–1945.
- Ghannoum O.** 2009. C<sub>4</sub> photosynthesis and water stress. *Annals of Botany* **103**, 635–644.
- Ghannoum O, Conroy JP.** 1998. Nitrogen deficiency precludes a growth response to CO<sub>2</sub> enrichment in C<sub>3</sub> and C<sub>4</sub> *Panicum* grasses. *Australian Journal of Plant Physiology* **25**, 627–636.
- Ghannoum O, von Caemmerer S, Barlow EWR, Conroy JP.** 1997. The effect of CO<sub>2</sub> enrichment and irradiance on the growth, morphology and gas exchange of a C<sub>3</sub> (*Panicum laxum*) and a C<sub>4</sub> (*Panicum antidotale*) grass. *Australian Journal of Plant Physiology* **24**, 227–237.
- Gillon JS, Yakir D.** 2000a. Internal conductance to CO<sub>2</sub> diffusion and C<sup>18</sup>O discrimination in C<sub>3</sub> leaves. *Plant Physiology* **123**, 201–214.
- Gillon JS, Yakir D.** 2000b. Naturally low carbonic anhydrase activity in C<sub>4</sub> and C<sub>3</sub> plants limits discrimination against C<sup>18</sup>O during photosynthesis. *Plant, Cell & Environment* **23**, 903–915.
- Gu L, Sun Y.** 2014. Artefactual responses of mesophyll conductance to CO<sub>2</sub> and irradiance estimated with the variable *J* and online isotope discrimination methods. *Plant, Cell & Environment* **37**, 1231–1249.



- Hassiotou F, Ludwig M, Renton M, Veneklaas EJ, Evans JR.** 2009. Influence of leaf dry mass per area, CO<sub>2</sub>, and irradiance on mesophyll conductance in sclerophylls. *Journal of Experimental Botany* **60**, 2303–2314.
- Hatch MD.** 1987. C<sub>4</sub> photosynthesis: a unique blend of modified biochemistry, anatomy and ultrastructure. *Biochemical and Biophysical Acta* **895**, 81–106.
- Hatch MD, Burnell JN.** 1990. Carbonic anhydrase activity in leaves and its role in the first step of C<sub>4</sub> photosynthesis. *Plant Physiology* **93**, 825–828.
- Hatch MD, Slack CR, Johnson HS.** 1967. Further studies on a new pathway of photosynthetic carbon dioxide fixation in sugar-cane and its occurrence in other plant species. *The Biochemical Journal* **102**, 417–422.
- Henderson SA, von Caemmerer S, Farquhar GD.** 1992. Short-term measurements of carbon isotope discrimination in several C<sub>4</sub> species. *Australian Journal of Plant Physiology* **19**, 263–285.
- Jenkins CL, Furbank RT, Hatch MD.** 1989. Mechanism of C<sub>4</sub> photosynthesis: a model describing the inorganic carbon pool in bundle sheath cells. *Plant Physiology* **91**, 1372–1381.
- Kolbe AR, Cousins AB.** 2018. Mesophyll conductance in *Zea mays* responds transiently to CO<sub>2</sub> availability: implications for transpiration efficiency in C<sub>4</sub> crops. *New Phytologist*. In press. doi:10.1111/nph.14942.
- Kromdijk J, Griffiths H, Schepers HE.** 2010. Can the progressive increase of C<sub>4</sub> bundle sheath leakiness at low PFD be explained by incomplete suppression of photorespiration? *Plant, Cell & Environment* **33**, 1935–1948.
- Kromdijk J, Ubierna N, Cousins AB, Griffiths H.** 2014. Bundle-sheath leakiness in C<sub>4</sub> photosynthesis: a careful balancing act between CO<sub>2</sub> concentration and assimilation. *Journal of Experimental Botany* **65**, 3443–3457.
- Leakey ADB, Bernacchi CJ, Dohleman FG, Ort DR, Long SP.** 2004. Will photosynthesis of maize (*Zea mays*) in the US Corn Belt increase in future [CO<sub>2</sub>] rich atmospheres? An analysis of diurnal courses of CO<sub>2</sub> uptake under free-air concentration enrichment (FACE). *Global Change Biology* **10**, 951–962.
- Loreto F, Harley PC, Di Marco G, Sharkey TD.** 1992. Estimation of mesophyll conductance to CO<sub>2</sub> flux by three different methods. *Plant Physiology* **98**, 1437–1443.
- Markelz RJ, Strellner RS, Leakey AD.** 2011. Impairment of C<sub>4</sub> photosynthesis by drought is exacerbated by limiting nitrogen and ameliorated by elevated [CO<sub>2</sub>] in maize. *Journal of Experimental Botany* **62**, 3235–3246.
- Osborn HL, Alonso-Cantabrana H, Sharwood RE, Covshoff S, Evans JR, Furbank RT, von Caemmerer S.** 2017. Effects of reduced carbonic anhydrase activity on CO<sub>2</sub> assimilation rates in *Setaria viridis*: a transgenic analysis. *Journal of Experimental Botany* **68**, 299–310.
- Peisker M.** 1986. Models of carbon metabolism in C<sub>3</sub>–C<sub>4</sub> intermediate plants as applied to the evolution of C<sub>4</sub> photosynthesis. *Plant, Cell & Environment* **9**, 627–635.
- Peisker M, Henderson SA.** 1992. Carbon: terrestrial C<sub>4</sub> plants. *Plant, Cell & Environment* **15**, 987–1004.
- Pengelly JJ, Sirault XR, Tazoe Y, Evans JR, Furbank RT, von Caemmerer S.** 2010. Growth of the C<sub>4</sub> dicot *Flaveria bidentis*: photosynthetic acclimation to low light through shifts in leaf anatomy and biochemistry. *Journal of Experimental Botany* **61**, 4109–4122.
- Sage RF.** 2004. The evolution of C<sub>4</sub> photosynthesis. *New Phytologist* **161**, 341–370.
- Steduto P, Katerji N, Puertos-Molina H, Ünlü M, Mastrorilli M, Rana G.** 1997. Water-use efficiency of sweet sorghum under water stress conditions. Gas-exchange investigations at leaf and canopy scales. *Field Crops Research* **54**, 221–234.
- Stryer L.** 1988. *Biochemistry*. New York: W. H. Freeman.
- Tazoe Y, von Caemmerer S, Badger MR, Evans JR.** 2009. Light and CO<sub>2</sub> do not affect the mesophyll conductance to CO<sub>2</sub> diffusion in wheat leaves. *Journal of Experimental Botany* **60**, 2291–2301.
- Tazoe Y, von Caemmerer S, Estavillo GM, Evans JR.** 2011. Using tunable diode laser spectroscopy to measure carbon isotope discrimination and mesophyll conductance to CO<sub>2</sub> diffusion dynamically at different CO<sub>2</sub> concentrations. *Plant, Cell & Environment* **34**, 580–591.
- Tholen D, Ethier G, Genty B, Pepin S, Zhu XG.** 2012. Variable mesophyll conductance revisited: theoretical background and experimental implications. *Plant, Cell & Environment* **35**, 2087–2103.
- Tholen D, Zhu XG.** 2011. The mechanistic basis of internal conductance: a theoretical analysis of mesophyll cell photosynthesis and CO<sub>2</sub> diffusion. *Plant Physiology* **156**, 90–105.
- Ubierna N, Gandin A, Boyd RA, Cousins AB.** 2017. Temperature response of mesophyll conductance in three C<sub>4</sub> species calculated with two methods: <sup>18</sup>O discrimination and in vitro V<sub>pmax</sub>. *New Phytologist* **214**, 66–80. Corrigendum. *New Phytologist* **217**: 956–959.
- Ubierna N, Sun W, Cousins AB.** 2011. The efficiency of C<sub>4</sub> photosynthesis under low light conditions: assumptions and calculations with CO<sub>2</sub> isotope discrimination. *Journal of Experimental Botany* **62**, 3119–3134.
- Ubierna N, Sun W, Kramer DM, Cousins AB.** 2013. The efficiency of C<sub>4</sub> photosynthesis under low light conditions in *Zea mays*, *Miscanthus × giganteus* and *Flaveria bidentis*. *Plant, Cell & Environment* **36**, 365–381.
- von Caemmerer S.** 2000. *Biochemical models of leaf photosynthesis*. Collingwood, Australia: CSIRO publishing.
- von Caemmerer S, Ghannoum O, Pengelly JJ, Cousins AB.** 2014. Carbon isotope discrimination as a tool to explore C<sub>4</sub> photosynthesis. *Journal of Experimental Botany* **65**, 3459–3470.
- Warren CR.** 2008. Stand aside stomata, another actor deserves centre stage: the forgotten role of the internal conductance to CO<sub>2</sub> transfer. *Journal of Experimental Botany* **59**, 1475–1487.
- Warren CR, Ethier GJ, Livingston NJ, Grant NJ, Turpin DH, Harrison DL, Black TA.** 2003. Transfer conductance in second growth Douglas-fir (*Pseudotsuga menziesii* (Mirb.) Franco) canopies. *Plant, Cell & Environment* **26**, 1215–1227.
- Yin X, van der Putten PE, Driever SM, Struik PC.** 2016. Temperature response of bundle-sheath conductance in maize leaves. *Journal of Experimental Botany* **67**, 2699–2714.